

UC Santa Cruz

UC Santa Cruz Previously Published Works

Title

Conformational Flexibility in Respiratory Syncytial Virus G Neutralizing Epitopes.

Permalink

<https://escholarship.org/uc/item/9d72d4bd>

Journal

Journal of Virology, 94(6)

ISSN

0022-538X

Authors

Fedechkin, Stanislav O

George, Natasha L

Nuñez Castrejon, Ana M

et al.

Publication Date

2020-02-28


DOI

10.1128/jvi.01879-19

Peer reviewed



Conformational Flexibility in Respiratory Syncytial Virus G Neutralizing Epitopes

Stanislav O. Fedechkin,^a Natasha L. George,^a Ana M. Nuñez Castrejon,^a Joshua R. Dillen,^a Lawrence M. Kauvar,^b  Rebecca M. DuBois^a

^aDepartment of Biomolecular Engineering, University of California—Santa Cruz, Santa Cruz, California, USA

^bTrellis Bioscience, LLC, Redwood City, California, USA

ABSTRACT Respiratory syncytial virus (RSV) is a top cause of severe lower respiratory tract disease and mortality in infants and the elderly. Currently, no vaccine or effective treatment exists for RSV. The RSV G glycoprotein mediates viral attachment to cells and contributes to pathogenesis by modulating host immunity through interactions with the human chemokine receptor CX3CR1. Antibodies targeting the RSV G central conserved domain are protective in both prophylactic and postinfection animal models. Here, we describe the crystal structure of the broadly neutralizing human monoclonal antibody 3G12 bound to the RSV G central conserved domain. Antibody 3G12 binds to a conformational epitope composed of highly conserved residues, explaining its broad neutralization activity. Surprisingly, RSV G complexed with 3G12 adopts a distinct conformation not observed in previously described RSV G-antibody structures. Comparison to other structures reveals that the RSV G central conserved domain is flexible and can adopt multiple conformations in the regions flanking the cysteine noose. We also show that restriction of RSV G flexibility with a proline mutation abolishes binding to antibody 3G12 but not antibody 3D3, which recognizes a different conformation of RSV G. Our studies provide new insights for rational vaccine design, indicating the importance of preserving both the global structural integrity of antigens and local conformational flexibility at antigenic sites, which may elicit a more diverse antibody response and broader protection against infection and disease.

IMPORTANCE Respiratory syncytial virus (RSV) causes severe respiratory infections in infants, young children, and the elderly, and currently, no licensed vaccine exists. In this study, we describe the crystal structure of the RSV surface glycoprotein G in complex with a broadly neutralizing human monoclonal antibody. The antibody binds to RSV G at a highly conserved region stabilized by two disulfide bonds, but it captures RSV G in a conformation not previously observed, revealing that this region is both structured and flexible. Importantly, our findings provide insight for the design of vaccines that elicit diverse antibodies, which may provide broad protection from infection and disease.

KEYWORDS X-ray crystallography, broadly neutralizing antibodies, protein structure-function, respiratory syncytial virus

Respiratory syncytial virus (RSV) is a globally prevalent virus that affects the airways and lungs. Infants and young children are at the highest risk of severe outcomes from RSV infection, with 33.1 million episodes of lower respiratory tract infection and approximately 3.2 million hospital visits and 118,200 deaths per year worldwide in children under the age of 5 years due to RSV (1). RSV is also a major cause of illness in adults older than 65 years of age and immunocompromised individuals, with an

Citation Fedechkin SO, George NL, Nuñez Castrejon AM, Dillen JR, Kauvar LM, DuBois RM. 2020. Conformational flexibility in respiratory syncytial virus G neutralizing epitopes. *J Virol* 94:e01879-19. <https://doi.org/10.1128/JVI.01879-19>.

Editor Rebecca Ellis Dutch, University of Kentucky College of Medicine

Copyright © 2020 American Society for Microbiology. All Rights Reserved.

Address correspondence to Rebecca M. DuBois, rmdubois@ucsc.edu.

Received 3 November 2019

Accepted 10 December 2019

Accepted manuscript posted online 18 December 2019

Published 28 February 2020

estimated 14,000 deaths per year in the United States (2). Hospitalization due to RSV is a major economic burden, especially in preterm infants and older adults (3).

Currently, no licensed vaccine exists for the prevention of RSV infection, making RSV one of the highest-burden diseases with no readily available preventative measure. The only FDA-approved therapy for RSV is passive prophylaxis with palivizumab (Synagis), a monoclonal antibody (mAb) that reduces disease severity and hospitalization (4). Palivizumab's approved use is limited to high-risk premature-birth infants; moreover, the high cost, approximately \$10,000 for a full course of therapy, limits use even in that narrow indication (5). The need for widely available vaccines and therapies for RSV is evidenced by the 19 vaccine candidates and therapeutic monoclonal antibodies in clinical trials (6).

RSV is a negative-sense single-stranded RNA virus with two major glycoproteins on the virion surface: the attachment glycoprotein (G) and the fusion glycoprotein (F) (7). RSV G is responsible for cellular attachment to host cells, and RSV F causes the viral membrane to fuse with the target host cell membrane. While both RSV F and G are immunogenic and are targeted by neutralizing antibodies, the majority of neutralizing antibodies in human sera target RSV F (8, 9). As such, most RSV vaccine candidates and therapeutic antibodies currently in development focus on RSV F. However, RSV that does not express the G protein is highly attenuated *in vivo* (10), and monoclonal antibodies that target RSV G are protective *in vivo* (11–21). In humans, anti-G antibodies are associated with lower clinical disease severity scores, despite an abundance in sera more than 30 times lower than anti-F antibodies (8). Thus, the RSV G protein is increasingly recognized as an important target for RSV vaccine and therapeutic antibody development (22).

RSV G is a type II membrane protein containing two mucin-like regions coated with 30 to 40 O-linked glycans and 3 to 5 N-linked glycans (Fig. 1A) (7, 23, 24). There are two forms of RSV G produced during infection. Membrane-bound RSV G is responsible for virus attachment to airway epithelial cells via the human chemokine receptor CX3CR1 (25–28). A secreted form of RSV G, derived from a second translation initiation site at Met48 and released from the membrane by proteolysis, is expressed early in infection (first ~6 h, prior to the release of virions at ~12 h) (Fig. 1A) (29). Secreted RSV G modulates signaling and trafficking of CX3CR1⁺ immune cells, contributing to airway congestion and pathogenesis (26, 27, 30–33). Between the two mucin-like regions of RSV G is a central conserved domain (CCD) of ~40 highly conserved amino acids, including 4 invariant cysteines forming a cysteine noose motif with two disulfide bonds (1-4, 2-3 connectivity) (Fig. 1A) (34–36). While the C terminus of the RSV G CCD possesses a heparin binding domain (Fig. 1A) (37, 38), initial RSV infection is thought to be mediated primarily by interactions between the RSV G CCD and CX3CR1 on ciliated airway cells (25–28), which do not have measurable heparan sulfate proteoglycans on their surfaces (39).

Broadly neutralizing monoclonal antibodies (bnmAbs) that target RSV G are able to neutralize RSV infectivity in cell culture, including in human airway epithelial (HAE) cells, and significantly reduce RSV viral loads and disease in both prophylactic and postinfection animal models (12, 14–16, 21, 25, 28, 40, 41). In addition, treatment with anti-RSV G mAbs reduces bronchoalveolar lavage (BAL) fluid cell influx, including RSV G protein-induced leukocyte migration and eosinophilic inflammatory responses, resulting in decreased airway congestion (15, 33, 42). Anti-G mAbs have also been shown to reduce mucus production and to restore beneficial antiviral alpha interferon (IFN- α) (18, 42–44). Most of the anti-G bnmAbs that have been studied to date bind with high affinity to RSV G (K_D [binding dissociation constant] = 1.1 pM to 3.3 nM) and bind to linear epitopes within the RSV G CCD as determined by linear epitope mapping techniques (17, 21, 40, 45). Recently, two studies elucidated four high-resolution crystal structures of antibody-RSV G CCD complexes (16, 46). Unexpectedly, all four antibodies have additional interactions outside their linear epitopes, revealing a previously unappreciated role of the disulfide-stabilized cysteine noose in forming conformational epitopes and contributing to high-affinity antibody binding.

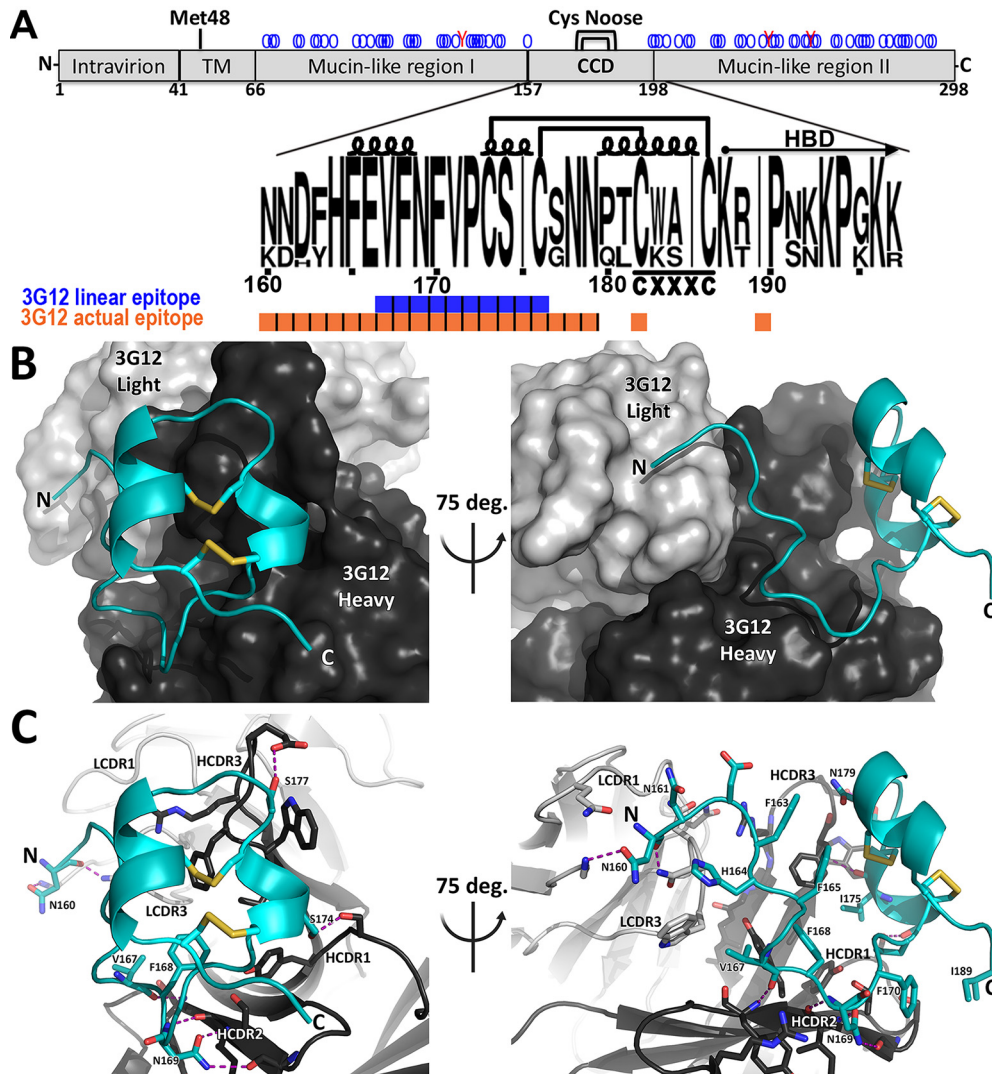


FIG 1 Crystal structure of the Fab 3G12-RSV G¹⁵⁷⁻¹⁹⁷ complex. (A) Schematic of the RSV G glycoprotein from RSV strain A2, including the transmembrane region (TM), the CCD, the cysteine noose (Cys noose), and the heparin binding domain (HBD). Met48 is the alternate initiation site for the production of soluble RSV G. Predicted N- and O-linked glycans are shown by red "Y's" and blue "O's," respectively. Below is a sequence logo of residues 160 to 197 of the RSV G CCD, revealing sequence conservation across strains RSV A, RSV B, RSV L, and RSV 1 to 8. (B) Overall views of the antibody 3G12 heavy chain (dark gray) and light chain (light gray) bound to RSV G¹⁵⁷⁻¹⁹⁷ (cyan, with disulfides in yellow). (C) Detailed views of interactions of antibody 3G12 with the RSV G CCD, with the same viewpoints as in panel B. Hydrogen bonds are shown as dashes. Heavy chain complementarity-determining regions (HCDR1 to -3) and light chain complementarity-determining regions (LCDR1 and -3) are labeled.

Here, we investigated the human bnmAb 3G12, which reduces viral loads, airway hyperresponsiveness, and inflammation in both prophylactic and postinfection mouse models of RSV infection (12, 21). Linear epitope mapping experiments have shown that bnmAb 3G12 binds to RSV G CCD residues 167 to 176, which is shifted downstream compared to other anti-G bnmAbs in the panel that bind primarily RSV G residues 162 to 169 (12, 21). We hypothesized that structural studies into the 3G12 epitope might reveal additional information about the mechanisms of high-affinity antibody binding and broad neutralization against RSV A and B strains. We present here the structure of antibody 3G12 bound to the RSV G CCD, which reveals a novel conformational epitope composed of highly conserved residues. Comparison to other structures highlights the flexible nature of the RSV G CCD. We furthermore show that RSV G flexibility is important for binding by antibody 3G12. Overall, these studies have broad implications for vaccine antigen design. The studies highlight the importance of preserving antigen

TABLE 1 Crystallographic data collection and refinement statistics

Parameter	Value(s) for Fab 3G12-RSV G ^{157–197b}
PDB accession no.	6UVO
Data collection statistics ^a	
Space group	P3 ₁ 21
Cell dimensions	
<i>a</i> , <i>b</i> , <i>c</i> (Å)	139.33, 139.33, 94.77
α , β , γ (°)	90, 90, 120
Resolution (Å)	74.53–2.90 (3.00–2.90)
Total no. of reflections	93,208 (14,475)
No. of unique reflections	23,682 (3,763)
R_{merge}^c	0.097 (0.641)
$I/\sigma(I)$	9.4 (1.9)
Completeness (%)	99.5 (99.5)
Redundancy	3.9 (3.8)
$CC_{1/2}^d$	0.993 (0.601)
Refinement statistics	
Resolution (Å)	74.53–2.90
No. of reflections	23,665
$R_{\text{work}}/R_{\text{free}}^e$	0.193/0.209
No. of atoms	
Protein	3,595
Ligand/ion	0
Water	0
<i>B</i> -factors (Å ²)	
Protein: bnmAb	62
Protein: RSV G	76
Ligand/ion	0
RMSD	
Bond lengths (Å)	0.015
Bond angles (°)	2.067
Ramachandran plot (%)	
Favored regions	95.7
Allowed regions	4.3
Outliers	0

^aData from one crystal were used.

^bValues in parentheses are for the highest-resolution shell.

^c $R_{\text{merge}} = \sum(|I - \langle I \rangle|) / \sum(I)$, where *I* is the observed intensity.

^d $CC_{1/2}$ is the Pearson correlation coefficient between random half-data sets.

^e $R_{\text{work}} = \sum \|F_o\| - |F_c| / \sum \|F_o\|$ for all data except 5%, which were used for R_{free} calculation.

structural integrity and also maintaining flexibility in antigenic sites, in order to elicit a diverse antibody response.

RESULTS

Fab 3G12-RSV G^{157–197} complex structure. We investigated bnmAb 3G12, a native human antibody that binds RSV G with high affinity, with a K_D of 579 pM. Antibody 3G12 shows broadly neutralizing activity across diverse laboratory and clinical RSV strains (21). To understand the molecular basis for the broad reactivity of bnmAb 3G12 and to determine if it binds to a larger conformational epitope beyond that predicted by linear epitope mapping, we used X-ray crystallographic studies to determine the structure of bnmAb 3G12 bound to the RSV G CCD (Fig. 1A). Purified antigen binding fragment (Fab) 3G12 was mixed with recombinant RSV G^{157–197}, which formed a stable complex in solution. We crystallized the Fab 3G12-RSV G^{157–197} complex and determined its crystal structure to a 2.9-Å resolution (Fig. 1B and C and Table 1).

The Fab 3G12-RSV G^{157–197} complex structure reveals a 924-Å² epitope on the RSV G CCD, with the 3G12 heavy chain burying 697 Å² and the light chain burying 227 Å² of the epitope (Fig. 1B). Similar to RSV G-antibody structures determined previously (16, 46), antibody 3G12 binds to a conformational epitope comprising RSV G residues 160 to 179, 182, and 189, revealing additional interactions beyond the linear epitope residues 167 to 176 (Fig. 1). Epitope residues are invariant or highly conserved (Fig. 1A),

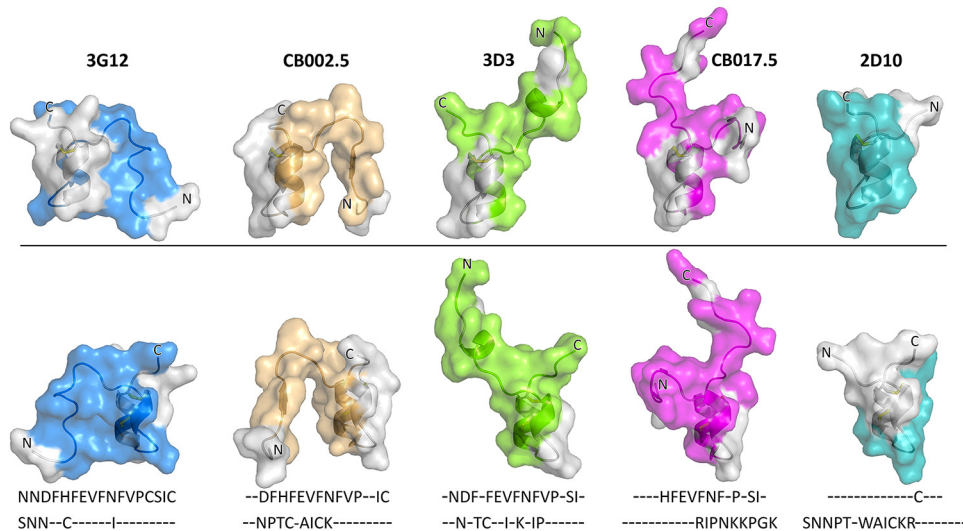


FIG 2 Comparison of known RSV G CCD epitopes and structures. Epitope amino acids interacting with antibodies are colored as follows: blue, 3G12; gold, CB002.5; green, 3D3; magenta, CB017.5; cyan, 2D10. Bottom panels are rotated 180° around the y axis compared to the top panels. Epitope amino acids were determined by the PDBePISA server and are indicated below each structure.

explaining the broad reactivity of bnmAb 3G12 for diverse RSV strains. The 3G12 heavy chain complementarity-determining regions (HCDRs) account for the majority of the interactions and buried surface with the RSV G CCD, with HCDR2 burying the largest portion, 315 Å², and HCDR3 accounting for 284 Å² (Fig. 1C). On the light chain complementarity-determining regions (LCDRs), LCDR3 buries 169.5 Å² on the N-terminal end of the RSV G CCD, while LCDR1 and the Fab 3G12 N-terminal residues form additional minor interactions (Fig. 1C). 3G12 heavy chain CDR2 stabilizes residues 167 to 170 of RSV G by several hydrogen bonds and van der Waals interactions (Fig. 1C). In addition, residues from all three of the HCDRs from bnmAb 3G12 stabilize hydrophobic interactions with RSV G residues F163, F165, F168, F170, P172, and I175, forming a hydrophobic core-like region within the antibody 3G12-RSV G complex (Fig. 1C). Interestingly, the helix on the C-terminal end of the cysteine noose, which encompasses the CX3C motif (residues 180 to 186), has almost no interactions with antibody 3G12, unlike other antibody-RSV G CCD structures where this helix has a role in antibody binding (Fig. 1C and Fig. 2).

RSV G CCD epitopes and conformational flexibility. To better understand the conformational flexibility in the RSV G CCD, all known structures of the CCD bound by antibodies were compared (Fig. 2). The structures were aligned at the cysteine noose region (residues ~170 to 187), which has a root mean square deviation (RMSD) of <0.6 Å across all structures. The region N terminal to the cysteine noose (residues ~160 to 169) adopts a different conformation in each structure (RMSD of 3 to 5 Å) and varies in secondary structural elements (i.e., it forms a helix when bound to antibody 3D3 and forms a strand when bound to antibody CB002.5) (Fig. 2). RSV G residue N169 appears to be flexible across all of the structures and may be one of the last ordered residues in the N-terminal region of the CCD. Similarly, the C-terminal region after K187 may be flexible and capable of adopting multiple conformations (Fig. 2). These C-terminal RSV G CCD residues are present in most of the complexes but do not have visible electron density, suggesting that they are dynamic and flexible. Overall, the RSV G CCD cysteine noose is structurally conserved and is an important structural element for antibody binding; however, the N- and C-terminal regions of the CCD are flexible and are captured in different conformations by diverse antibodies.

Role of RSV G flexibility in bnmAb binding. To evaluate the role of RSV G flexibility in bnmAb binding, we sought to investigate a mutant of RSV G with restricted

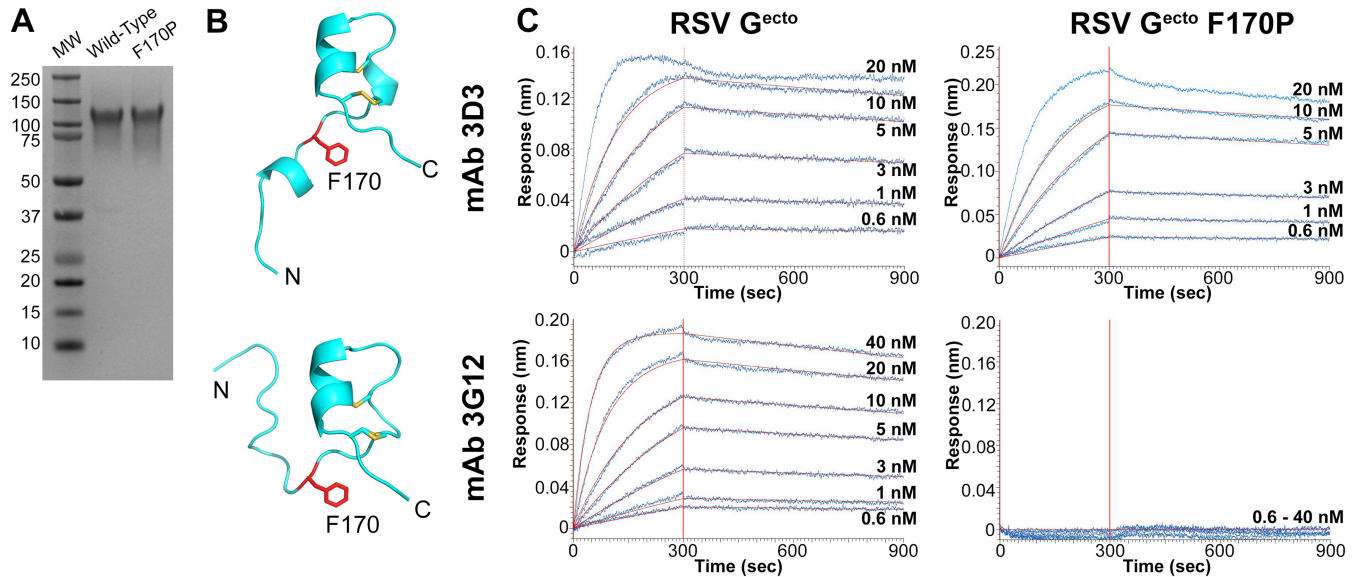


FIG 3 Differences in bnmAb 3G12 and bnmAb 3D3 binding to RSV G^{ecto} F170P. (A) Coomassie-stained SDS-polyacrylamide gel of RSV G^{ecto} (wild type) and RSV G^{ecto} F170P (F170P). Molecular weight (MW) ladder values (in kilodaltons) are labeled. (B) Structure of the RSV G CCD when bound to bnmAb 3D3 (top) and bnmAb 3G12 (bottom). F170 is in red. (C) Biolayer interferometry traces (blue) and curve fits (red) for binding of bnmAb 3D3 (top) and bnmAb 3G12 (bottom) to RSV G^{ecto} and RSV G^{ecto} F170P. Concentrations of G^{ecto} used for each trace are shown. The vertical red line indicates the transition of the biosensors from the association step to the dissociation step. Binding on-rates, off-rates, dissociation constants, and curve fit statistics are shown in Table 2.

flexibility in its CCD. We chose the F170P mutant, which was previously identified among neutralization escape mutants of respiratory syncytial virus grown in the presence of an anti-G monoclonal antibody (47). The F170 side chain contributes only 1.3% of the 3G12 epitope (12 \AA^2 of the 924 \AA^2), suggesting that mutation of the side chain alone would not substantially affect bnmAb 3G12 binding. However, when bound to bnmAb 3G12, RSV G residue F170 has a Phi torsion angle of -143° , whereas a typical proline is restricted to a Phi torsion angle of -60° . Thus, we reasoned that the proline mutation would restrict the flexibility of the RSV G CCD and could affect bnmAb binding. We produced and purified the wild-type RSV G ectodomain (RSV G^{ecto}) and its mutant (RSV G^{ecto} F170P) (Fig. 3A). We then evaluated binding by bnmAbs 3G12 and 3D3, which bind to two very different conformations of the RSV G CCD (Fig. 3B). Biolayer interferometry binding studies reveal that while both bnmAbs bind to wild-type RSV G^{ecto} with high affinity, bnmAb 3G12, but not 3D3, completely lost binding to the mutant RSV G^{ecto} F170P (Fig. 3C and Table 2). These data reveal that the mutant RSV G^{ecto} F170P can adopt the conformation for the 3D3 epitope; however, it cannot adopt the conformation for the 3G12 epitope.

DISCUSSION

Our study highlights how even disulfide-constrained antigens can have flexible, dynamic antigenic sites and that different high-affinity antibodies can target these sites in distinct ways. We describe the crystal structure of the human bnmAb 3G12 bound to the RSV G CCD and show that bnmAb 3G12 binding is dependent on RSV G flexibility. The antibody binds to a conformational epitope composed of highly conserved resi-

TABLE 2 Biolayer interferometry binding studies^a

Sample	bnmAb	Mean K_D (pM) (SE)	Mean k_a ($10^5 \text{ M}^{-1} \text{ s}^{-1}$) (SE)	Mean k_d (10^{-4} s^{-1}) (SE)	R^2
RSV G^{ecto}	3D3	202 (± 1)	8.73 (± 0.02)	1.77 (± 0.01)	0.998
RSV G^{ecto} F170P	3D3	264 (± 1)	6.23 (± 0.01)	1.65 (± 0.01)	0.999
RSV G^{ecto}	3G12	423 (± 1)	5.27 (± 0.01)	2.23 (± 0.01)	0.999
RSV G^{ecto} F170P	3G12	NB			

^a K_D , binding dissociation constant; k_a , on-rate; k_d , off-rate; R^2 , curve fit statistic; NB, no binding observed. Values in parentheses are standard errors.

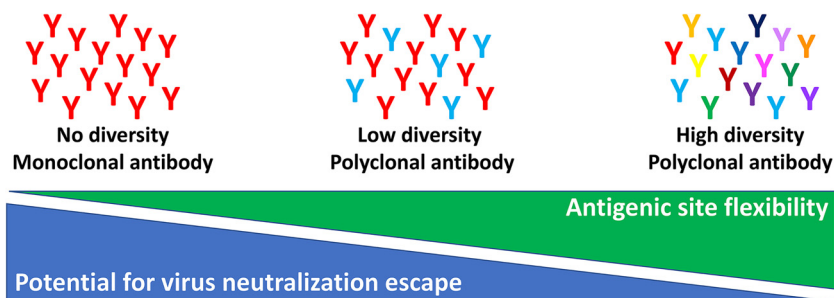


FIG 4 Proposed model relating antigenic site flexibility, antibody response diversity for that site, and the potential for virus neutralization escape at that site.

dues, explaining its broad reactivity to diverse strains of RSV. The antibody interacts mainly with the RSV G CCD's N-terminal region, in a conformation distinct from those of all other known CCD structures, suggesting that the RSV G CCD is flexible outside its rigid disulfide-bonded cysteine noose region. Residue N169 likely represents a “hinge” residue, where the N-terminal region of the CCD preceding N169 appears to be flexible and capable of adopting multiple conformations and even secondary structures. Likewise, residues after K187 in the C-terminal region of the CCD also appear to be flexible. Thus, RSV G is part of a growing list of antigens with flexible or intrinsically disordered regions (IDRs) that are targeted by antibodies (48–56).

The observation of different conformations of the RSV G CCD raises several important questions. Does RSV G move freely and randomly, and do our structures reveal momentary snapshots captured by antibody binding? What conformation does RSV G adopt when interacting with the human CX3CR1 receptor? We note that none of the conformations have any substantial tertiary-structure-stabilizing interactions within the CCD or clearly defined secondary structure. Therefore, it is unlikely that RSV G assumes distinct conformations without additional external stabilizing interactions. One form of stabilization may come from the oligomerization state of RSV G. It was previously suggested that RSV G exists as a trimer or tetramer (57, 58). The extensive glycosylation of RSV G in the mucin-like regions flanking the CCD may also restrict RSV G flexibility. It is also possible that RSV G interacts with RSV F on the virus surface, creating a quaternary structure that may limit RSV G to defined structures like those captured by the antibodies discussed in this paper. Interestingly, in an RSV virus-like particle vaccine containing F and G, the conformation of F affected the immunogenicity of G (59). These factors may be important in the design of an RSV vaccine.

Our study also has important implications for vaccine antigen design in a broader sense. Recently, there has been a trend to stabilize antigens based on structural analyses to elicit higher levels of neutralizing antibodies targeting specific epitopes, e.g., HIV gp120, influenza virus hemagglutinin, Middle East respiratory syndrome (MERS) coronavirus spike, human parainfluenza virus fusion protein, human metapneumovirus fusion protein, and RSV fusion protein (60–71). A common approach to antigen stabilization in many of the above-mentioned studies involves the introduction of proline substitutions and disulfide bonds, which can stabilize by limiting polypeptide backbone mobility. However, antigen overstabilization could limit the diversity of antibody responses. In support of this concept, we show that limiting the flexibility of RSV G with a proline mutation abolishes the epitope for the high-affinity bnmAb 3G12. Thus, when designing stabilized antigens that display specific epitopes, one should also consider the benefits of preserving the native flexibility of antigenic sites, which may elicit a more diverse immune response and may offer better protection against virus escape (Fig. 4). Incorporating antibody repertoire analysis technologies during vaccine development could provide opportunities to evaluate antibody diversity that is elicited by stabilized antigens.

MATERIALS AND METHODS

Production of bnmAb 3G12 and Fab 3G12. Recombinant bnmAb 3G12 was produced by transient transfection in CHO cells and purification by immobilized protein A, as described previously (21, 45). Fab 3G12 was generated by incubation of bnmAb 3G12 with immobilized papain, followed by the removal of the Fc fragment with immobilized protein A. Fab 3G12 was then purified by Superdex 200 size exclusion chromatography in a solution containing 10 mM Tris-HCl (pH 8.0) and 150 mM NaCl.

Expression and purification of RSV G¹⁵⁷⁻¹⁹⁷. A synthetic gene codon optimized for *Escherichia coli* encoding RSV G (strain A2) amino acids 157 to 197 (UniProtKB accession number [P03423](#)) with a C-terminal six-histidine purification tag was cloned into pET52b. Recombinant RSV G¹⁵⁷⁻¹⁹⁷ was expressed overnight in *E. coli* BL21(DE3) at 18°C. *E. coli* cells were lysed by ultrasonication in a buffer containing 20 mM Tris-HCl (pH 8.0), 150 mM NaCl, and 25 mM imidazole (buffer A) with 2 μM MgCl₂, Benzonase, and protease inhibitors. RSV G¹⁵⁷⁻¹⁹⁷ was purified from soluble lysates by HisTrap FF affinity chromatography and eluted with a gradient into buffer B (buffer A containing 500 mM imidazole).

Formation and structure determination of the Fab 3G12-RSV G¹⁵⁷⁻¹⁹⁷ complex. Purified RSV G¹⁵⁷⁻¹⁹⁷ was mixed in a 2-fold molar excess with purified Fab 3G12, incubated for 1 h at 4°C, and purified by Superdex 75 size exclusion chromatography in a solution containing 10 mM Tris-HCl (pH 8.0) and 150 mM NaCl. The Fab 3G12-RSV G¹⁵⁷⁻¹⁹⁷ complex was concentrated to 15 mg/ml. Crystals were grown by hanging-drop vapor diffusion at 22°C with a well solution of 1.8 M ammonium sulfate and 100 mM sodium acetate trihydrate (pH 4.4). Crystals were transferred into a cryoprotectant solution of 2.0 M ammonium sulfate, 100 mM sodium acetate trihydrate (pH 4.4), and 25% glycerol and flash-frozen in liquid nitrogen. Diffraction data were collected at cryogenic temperature at the Advanced Light Source on beamline 8.3.1 using a wavelength of 1.11503 Å. Diffraction data from a single crystal were processed with iMosflm (72) and Aimless (73) (Table 1). The Fab 3G12-RSV G¹⁵⁷⁻¹⁹⁷ complex structure was solved by molecular replacement with the Fab under PDB accession number [5K59](#) and the program PHASER (74), and the structure was refined and manually rebuilt using PHENIX (75) and Coot (76), respectively (Table 1).

Expression and purification of RSV G^{ecto} and RSV G^{ecto} F170P. A codon-optimized synthetic gene encoding RSV G (strain A2) amino acids 64 to 298 (UniProtKB accession number [P03423](#)) was cloned into pCF in frame with an N-terminal CCR5 signal sequence, a C-terminal His tag, and Twin-Strep purification tags. The F170P mutation was introduced by Phusion site-directed mutagenesis and verified by Sanger sequencing. Recombinant RSV G^{ecto} and RSV G^{ecto} F170P were produced by transient transfection in HEK293F cells with Effectene transfection reagent (Qiagen). After 5 days, cell medium was supplemented with BioLock (IBA) and 20 mM Tris-HCl (pH 8.0) and 0.22-μm filtered. RSV G^{ecto} and RSV G^{ecto} F170P were batch purified from medium with Strep-Tactin resin (IBA), washed, and eluted with Strep-Tactin elution buffer (50 mM Tris [pH 8.0], 150 mM NaCl, 1 mM EDTA, 2.5 mM desthiobiotin). RSV G^{ecto} and RSV G^{ecto} F170P were concentrated and dialyzed into phosphate-buffered saline (PBS) using 10-kDa spin concentrators. Protein purity was evaluated by SDS-polyacrylamide gel electrophoresis.

Binding affinity analyses. An Octet RED96e biolayer interferometry instrument was used to evaluate the binding of bnmAbs 3G12 and 3D3 to RSV G^{ecto} and RSV G^{ecto} F170P. Antibody 3G12 or 3D3 at 1 μg/ml in Octet buffer (phosphate-buffered saline [pH 7.4], 0.05% Tween 20, 1% bovine serum albumin [BSA]) was loaded onto anti-human IgG Fc capture (AHC) biosensors, and 2-fold serially diluted RSV G^{ecto} or RSV G^{ecto} F170P, from 40 nM to 0.625 nM, was assessed for binding. Red lines are the fit of global association and dissociation with a 1:1 model, with at least 5 curves used to determine binding on- and off-rates and to calculate dissociation constants.

Data availability. Coordinates and structure factors have been deposited in the Protein Data Bank under accession number [6UVO](#).

ACKNOWLEDGMENTS

We thank Sarvind Tripathi for assistance in crystallographic data collection. We thank Edgar Tenorio for reviewing the manuscript.

R.M.D. is supported by National Institute of Allergy and Infectious Diseases (NIAID) grants R21AI130605 and R56AI141537. L.M.K. acknowledges partial support from NIAID grant 5R44AI122360-02. This research used resources of the Advanced Light Source (ALS), which is a U.S. Department of Energy (DOE) Office of Science User Facility under contract no. DE-AC02-05CH11231. Beamline 8.3.1 at the Advanced Light Source is operated by the University of California Office of the President, Multicampus Research Programs and Initiatives, grant MR-15-328599; the National Institutes of Health (R01 GM124149 and P30 GM124169); and Plexxikon Inc.

REFERENCES

- Shi T, McAllister DA, O'Brien KL, Simoes EAF, Madhi SA, Gessner BD, Polack FP, Balsells E, Acacio S, Aguayo C, Alassani I, Ali A, Antonio M, Awasthi S, Awori JO, Azziz-Baumgartner E, Baggett HC, Baillie VL, Balmaseda A, Barahona A, Basnet S, Bassat Q, Basualdo W, Bigogo G, Bont L, Breiman RF, Brooks WA, Broor S, Bruce N, Bruden D, Buchy P, Campbell S, Carosone-Link P, Chadha M, Chipeta J, Chou M, Clara W, Cohen C, de Cuellar E, Dang DA, Dash-Yandag B, Deloria-Knoll M, Dherani M, Eap T, Ebruke BE, Echavarría M, de Freitas Lazaro Emediato CC, Fasce RA, Feikin DR, Feng L, et al. 2017. Global, regional, and national disease burden estimates of acute lower respiratory infections due to respiratory syncytial virus in young children in

- 2015: a systematic review and modelling study. *Lancet* 390:946–958. [https://doi.org/10.1016/S0140-6736\(17\)30938-8](https://doi.org/10.1016/S0140-6736(17)30938-8).
2. Falsey AR, Hennessey PA, Formica MA, Cox C, Walsh EE. 2005. Respiratory syncytial virus infection in elderly and high-risk adults. *N Engl J Med* 352:1749–1759. <https://doi.org/10.1056/NEJMoa043951>.
 3. Amand C, Tong S, Kieffer A, Kyaw MH. 2018. Healthcare resource use and economic burden attributable to respiratory syncytial virus in the United States: a claims database analysis. *BMC Health Serv Res* 18:294. <https://doi.org/10.1186/s12913-018-3066-1>.
 4. Anonymous. 1998. Palivizumab, a humanized respiratory syncytial virus monoclonal antibody, reduces hospitalization from respiratory syncytial virus infection in high-risk infants. *Pediatrics* 102:531–537. <https://doi.org/10.1542/peds.102.3.531>.
 5. Meissner HC, Kimberlin DW. 2013. RSV immunoprophylaxis: does the benefit justify the cost? *Pediatrics* 132:915–918. <https://doi.org/10.1542/peds.2013-2449>.
 6. Mazur NI, Higgins D, Nunes MC, Melero JA, Langedijk AC, Horsley N, Buchholz UJ, Openshaw PJ, McLellan JS, Englund JA, Mejias A, Karron RA, Simoes EA, Knezevic I, Ramilo O, Piedra PA, Chu HY, Falsey AR, Nair H, Kragten-Tabatabaie L, Greenough A, Baraldi E, Papadopoulos NG, Vekeermans J, Polack FP, Powell M, Satav A, Walsh EE, Stein RT, Graham BS, Bont LJ, Respiratory Syncytial Virus Network Foundation. 2018. The respiratory syncytial virus vaccine landscape: lessons from the graveyard and promising candidates. *Lancet Infect Dis* 18:e295–e311. [https://doi.org/10.1016/S1473-3099\(18\)30292-5](https://doi.org/10.1016/S1473-3099(18)30292-5).
 7. McLellan JS, Ray WC, Peeples ME. 2013. Structure and function of respiratory syncytial virus surface glycoproteins. *Curr Top Microbiol Immunol* 372:83–104. https://doi.org/10.1007/978-3-642-38919-1_4.
 8. Capella C, Chaiwatpongakorn S, Gorrell E, Risch ZA, Ye F, Mertz SE, Johnson SM, Moore-Clingenpeel M, Ramilo O, Mejias A, Peeples ME. 2017. Prefusion F, postfusion F, G antibodies and disease severity in infants and young children with acute respiratory syncytial virus infection. *J Infect Dis* 216:1398–1406. <https://doi.org/10.1093/infdis/jix489>.
 9. Ngwuta JO, Chen M, Modjarrad K, Joyce MG, Kanekiyo M, Kumar A, Yassine HM, Moin SM, Killikelly AM, Chuang GY, Druz A, Georgiev IS, Rundlet EJ, Sastry M, Stewart-Jones GB, Yang Y, Zhang B, Nason MC, Capella C, Peeples ME, Ledgerwood JE, McLellan JS, Kwong PD, Graham BS. 2015. Prefusion F-specific antibodies determine the magnitude of RSV neutralizing activity in human sera. *Sci Transl Med* 7:309ra162. <https://doi.org/10.1126/scitranslmed.aac4241>.
 10. Teng MN, Whitehead SS, Collins PL. 2001. Contribution of the respiratory syncytial virus G glycoprotein and its secreted and membrane-bound forms to virus replication in vitro and in vivo. *Virology* 289:283–296. <https://doi.org/10.1006/viro.2001.1138>.
 11. Techaarpornkul S, Barretto N, Peeples ME. 2001. Functional analysis of recombinant respiratory syncytial virus deletion mutants lacking the small hydrophobic and/or attachment glycoprotein gene. *J Virol* 75:6825–6834. <https://doi.org/10.1128/JVI.75.15.6825-6834.2001>.
 12. Han J, Takeda K, Wang M, Zeng W, Jia Y, Shiraishi Y, Okamoto M, Dakhama A, Gelfand EW. 2014. Effects of anti-G and anti-F antibodies on airway function after respiratory syncytial virus infection. *Am J Respir Cell Mol Biol* 51:143–154. <https://doi.org/10.1165/rcmb.2013-0360OC>.
 13. Boyoglu-Barnum S, Todd SO, Chirkova T, Barnum TR, Gaston KA, Haynes LM, Tripp RA, Moore ML, Anderson LJ. 2015. An anti-G protein monoclonal antibody treats RSV disease more effectively than an anti-F monoclonal antibody in BALB/c mice. *Virology* 483:117–125. <https://doi.org/10.1016/j.virol.2015.02.035>.
 14. Boyoglu-Barnum S, Chirkova T, Todd SO, Barnum TR, Gaston KA, Jorquera P, Haynes LM, Tripp RA, Moore ML, Anderson LJ. 2014. Prophylaxis with a respiratory syncytial virus (RSV) anti-G protein monoclonal antibody shifts the adaptive immune response to RSV rA2-line19F infection from Th2 to Th1 in BALB/c mice. *J Virol* 88:10569–10583. <https://doi.org/10.1128/JVI.01503-14>.
 15. Boyoglu-Barnum S, Gaston KA, Todd SO, Boyoglu C, Chirkova T, Barnum TR, Jorquera P, Haynes LM, Tripp RA, Moore ML, Anderson LJ. 2013. A respiratory syncytial virus (RSV) anti-G protein F(ab')₂ monoclonal antibody suppresses mucous production and breathing effort in RSV rA2-line19F-infected BALB/c mice. *J Virol* 87:10955–10967. <https://doi.org/10.1128/JVI.01164-13>.
 16. Jones HG, Ritschel T, Pascual G, Brakenhoff JPJ, Keogh E, Furmanova-Hollenstein P, Lanckacker E, Wadia JS, Gilman MSA, Williamson RA, Roymans D, van 't Wout AB, Langedijk JP, McLellan JS. 2018. Structural basis for recognition of the central conserved region of RSV G by neutralizing human antibodies. *PLoS Pathog* 14:e1006935. <https://doi.org/10.1371/journal.ppat.1006935>.
 17. Lee HJ, Lee JY, Park MH, Kim JY, Chang J. 2017. Monoclonal antibody against G glycoprotein increases respiratory syncytial virus clearance in vivo and prevents vaccine-enhanced diseases. *PLoS One* 12:e0169139. <https://doi.org/10.1371/journal.pone.0169139>.
 18. Miao C, Radu GU, Caidi H, Tripp RA, Anderson LJ, Haynes LM. 2009. Treatment with respiratory syncytial virus G glycoprotein monoclonal antibody or F(ab')₂ components mediates reduced pulmonary inflammation in mice. *J Gen Virol* 90:1119–1123. <https://doi.org/10.1099/vir.0.009308-0>.
 19. Radu GU, Caidi H, Miao C, Tripp RA, Anderson LJ, Haynes LM. 2010. Prophylactic treatment with a G glycoprotein monoclonal antibody reduces pulmonary inflammation in respiratory syncytial virus (RSV)-challenged naive and formalin-inactivated RSV-immunized BALB/c mice. *J Virol* 84:9632–9636. <https://doi.org/10.1128/JVI.00451-10>.
 20. Caidi H, Harcourt JL, Tripp RA, Anderson LJ, Haynes LM. 2012. Combination therapy using monoclonal antibodies against respiratory syncytial virus (RSV) G glycoprotein protects from RSV disease in BALB/c mice. *PLoS One* 7:e51485. <https://doi.org/10.1371/journal.pone.0051485>.
 21. Collarini EJ, Lee FE, Foord O, Park M, Sperinde G, Wu H, Harriman WD, Carroll SF, Ellsworth SL, Anderson LJ, Tripp RA, Walsh EE, Keyt BA, Kauvar LM. 2009. Potent high-affinity antibodies for treatment and prophylaxis of respiratory syncytial virus derived from B cells of infected patients. *J Immunol* 183:6338–6345. <https://doi.org/10.4049/jimmunol.0901373>.
 22. Tripp RA, Power UF, Openshaw PJM, Kauvar LM. 2018. Respiratory syncytial virus: targeting the G protein provides a new approach for an old problem. *J Virol* 92:e01302-17. <https://doi.org/10.1128/JVI.01302-17>.
 23. Satake M, Coligan JE, Elango N, Norrby E, Venkatesan S. 1985. Respiratory syncytial virus envelope glycoprotein (G) has a novel structure. *Nucleic Acids Res* 13:7795–7812. <https://doi.org/10.1093/nar/13.21.7795>.
 24. Wertz GW, Collins PL, Huang Y, Gruber C, Levine S, Ball LA. 1985. Nucleotide sequence of the G protein gene of human respiratory syncytial virus reveals an unusual type of viral membrane protein. *Proc Natl Acad Sci U S A* 82:4075–4079. <https://doi.org/10.1073/pnas.82.12.4075>.
 25. Johnson SM, McNally BA, Ioannidis I, Flano E, Teng MN, Oomens AG, Walsh EE, Peeples ME. 2015. Respiratory syncytial virus uses CX3CR1 as a receptor on primary human airway epithelial cultures. *PLoS Pathog* 11:e1005318. <https://doi.org/10.1371/journal.ppat.1005318>.
 26. Tripp RA, Jones LP, Haynes LM, Zheng H, Murphy PM, Anderson LJ. 2001. CX3C chemokine mimicry by respiratory syncytial virus G glycoprotein. *Nat Immunol* 2:732–738. <https://doi.org/10.1038/90675>.
 27. Chirkova T, Lin S, Oomens AG, Gaston KA, Boyoglu-Barnum S, Meng J, Stobart CC, Cotton CU, Hartert TV, Moore ML, Ziady AG, Anderson LJ. 2015. CX3CR1 is an important surface molecule for respiratory syncytial virus infection in human airway epithelial cells. *J Gen Virol* 96:2543–2556. <https://doi.org/10.1099/vir.0.000218>.
 28. Jeong KI, Piepenhagen PA, Kishko M, DiNapoli JM, Groppo RP, Zhang L, Almond J, Kleanthous H, Delagrave S, Parrington M. 2015. CX3CR1 is expressed in differentiated human ciliated airway cells and co-localizes with respiratory syncytial virus on cilia in a G protein-dependent manner. *PLoS One* 10:e0130517. <https://doi.org/10.1371/journal.pone.0130517>.
 29. Bukreyev A, Yang L, Fricke J, Cheng L, Ward JM, Murphy BR, Collins PL. 2008. The secreted form of respiratory syncytial virus G glycoprotein helps the virus evade antibody-mediated restriction of replication by acting as an antigen decoy and through effects on Fc receptor-bearing leukocytes. *J Virol* 82:12191–12204. <https://doi.org/10.1128/JVI.01604-08>.
 30. Chirkova T, Boyoglu-Barnum S, Gaston KA, Malik FM, Trau SP, Oomens AG, Anderson LJ. 2013. Respiratory syncytial virus G protein CX3C motif impairs human airway epithelial and immune cell responses. *J Virol* 87:13466–13479. <https://doi.org/10.1128/JVI.01741-13>.
 31. Harcourt J, Alvarez R, Jones LP, Henderson C, Anderson LJ, Tripp RA. 2006. Respiratory syncytial virus G protein and G protein CX3C motif adversely affect CX3CR1 + T cell responses. *J Immunol* 176:1600–1608. <https://doi.org/10.4049/jimmunol.176.3.1600>.
 32. Arnold R, Konig B, Werchau H, Konig W. 2004. Respiratory syncytial virus deficient in soluble G protein induced an increased proinflammatory response in human lung epithelial cells. *Virology* 330:384–397. <https://doi.org/10.1016/j.virol.2004.10.004>.
 33. Haynes LM, Jones LP, Barskey A, Anderson LJ, Tripp RA. 2003. Enhanced disease and pulmonary eosinophilia associated with formalin-inactivated respiratory syncytial virus vaccination are linked to G glyco-

- protein CX3C-CX3CR1 interaction and expression of substance P. *J Virol* 77:9831–9844. <https://doi.org/10.1128/jvi.77.18.9831-9844.2003>.
34. Sugawara M, Czaplicki J, Ferrage J, Haeuw JF, Power UF, Corvaia N, Nguyen T, Beck A, Milton A. 2002. Structure-antigenicity relationship studies of the central conserved region of human respiratory syncytial virus protein G. *J Pept Res* 60:271–282. <https://doi.org/10.1034/j.1399-3011.2002.21027.x>.
 35. Langedijk JP, de Groot BL, Berendsen HJ, van Oirschot JT. 1998. Structural homology of the central conserved region of the attachment protein G of respiratory syncytial virus with the fourth subdomain of 55-kDa tumor necrosis factor receptor. *Virology* 243:293–302. <https://doi.org/10.1006/viro.1998.9066>.
 36. Doreleijers JF, Langedijk JP, Hard K, Boelens R, Rullmann JA, Schaaper WM, van Oirschot JT, Kaptein R. 1996. Solution structure of the immunodominant region of protein G of bovine respiratory syncytial virus. *Biochemistry* 35:14684–14688. <https://doi.org/10.1021/bi9621627>.
 37. Feldman SA, Hendry RM, Beeler JA. 1999. Identification of a linear heparin binding domain for human respiratory syncytial virus attachment glycoprotein G. *J Virol* 73:6610–6617. <https://doi.org/10.1128/JVI.73.8.6610-6617.1999>.
 38. Hallak LK, Collins PL, Knudson W, Peeples ME. 2000. Iduronic acid-containing glycosaminoglycans on target cells are required for efficient respiratory syncytial virus infection. *Virology* 271:264–275. <https://doi.org/10.1006/viro.2000.0293>.
 39. Zhang L, Bukreyev A, Thompson CI, Watson B, Peeples ME, Collins PL, Pickles RJ. 2005. Infection of ciliated cells by human parainfluenza virus type 3 in an in vitro model of human airway epithelium. *J Virol* 79:1113–1124. <https://doi.org/10.1128/JVI.79.2.1113-1124.2005>.
 40. Cortjens B, Yasuda E, Yu X, Wagner K, Claassen YB, Bakker AQ, van Woensel JBM, Beaumont T. 2017. Broadly reactive anti-respiratory syncytial virus G antibodies from exposed individuals effectively inhibit infection of primary airway epithelial cells. *J Virol* 91:e02357-16. <https://doi.org/10.1128/JVI.02357-16>.
 41. Lee J, Klenow L, Coyle EM, Golding H, Khurana S. 2018. Protective antigenic sites in respiratory syncytial virus G attachment protein outside the central conserved and cysteine noose domains. *PLoS Pathog* 14:e1007262. <https://doi.org/10.1371/journal.ppat.1007262>.
 42. Haynes LM, Caidi H, Radu GU, Miao C, Harcourt JL, Tripp RA, Anderson LJ. 2009. Therapeutic monoclonal antibody treatment targeting respiratory syncytial virus (RSV) G protein mediates viral clearance and reduces the pathogenesis of RSV infection in BALB/c mice. *J Infect Dis* 200:439–447. <https://doi.org/10.1086/600108>.
 43. Boyoglu-Barnum S, Todd SO, Meng J, Barnum TR, Chirkova T, Haynes LM, Jadhao SJ, Tripp RA, Oomens AG, Moore ML, Anderson LJ. 2017. Mutating the CX3C motif in the G protein should make a live respiratory syncytial virus vaccine safer and more effective. *J Virol* 91:e02059-16. <https://doi.org/10.1128/JVI.02059-16>.
 44. Shingai M, Azuma M, Ebihara T, Sasai M, Funami K, Ayata M, Ogura H, Tsutsumi H, Matsumoto M, Seya T. 2008. Soluble G protein of respiratory syncytial virus inhibits Toll-like receptor 3/4-mediated IFN-beta induction. *Int Immunol* 20:1169–1180. <https://doi.org/10.1093/intimm/dxn074>.
 45. Kauvar LM, Collarini EJA, Keyt BA, Foord OA. September 2012. Anti-RSV G protein antibodies. US patent 8,273,354.
 46. Fedechkin SO, George NL, Wolff JT, Kauvar LM, DuBois RM. 2018. Structures of respiratory syncytial virus G antigen bound to broadly neutralizing antibodies. *Sci Immunol* 3:eaar3534. <https://doi.org/10.1126/sciimmunol.aar3534>.
 47. Walsh EE, Falsey AR, Sullender WM. 1998. Monoclonal antibody neutralization escape mutants of respiratory syncytial virus with unique alterations in the attachment (G) protein. *J Gen Virol* 79(Part 3):479–487. <https://doi.org/10.1099/0022-1317-79-3-479>.
 48. MacRaidl CA, Richards JS, Anders RF, Norton RS. 2016. Antibody recognition of disordered antigens. *Structure* 24:148–157. <https://doi.org/10.1016/j.str.2015.10.028>.
 49. Chu HM, Wright J, Chan YH, Lin CJ, Chang TW, Lim C. 2014. Two potential therapeutic antibodies bind to a peptide segment of membrane-bound IgE in different conformations. *Nat Commun* 5:3139. <https://doi.org/10.1038/ncomms4139>.
 50. Yagi M, Bang G, Tougan T, Palapac NM, Arisue N, Aoshi T, Matsumoto Y, Ishii KJ, Egwang TG, Druilhe P, Horii T. 2014. Protective epitopes of the Plasmodium falciparum SERA5 malaria vaccine reside in intrinsically unstructured N-terminal repetitive sequences. *PLoS One* 9:e98460. <https://doi.org/10.1371/journal.pone.0098460>.
 51. Deng L, Ma L, Virata-Theimer ML, Zhong L, Yan H, Zhao Z, Struble E, Feinstone S, Alter H, Zhang P. 2014. Discrete conformations of epitope II on the hepatitis C virus E2 protein for antibody-mediated neutralization and nonneutralization. *Proc Natl Acad Sci U S A* 111:10690–10695. <https://doi.org/10.1073/pnas.1411317111>.
 52. Bogdanoff WA, Perez El, Lopez T, Arias CF, DuBois RM. 2018. Structural basis for escape of human astrovirus from antibody neutralization: broad implications for rational vaccine design. *J Virol* 92:e01546-17. <https://doi.org/10.1128/JVI.01546-17>.
 53. Jones HG, Battles MB, Lin CC, Bianchi S, Corti D, McLellan JS. 2019. Alternative conformations of a major antigenic site on RSV F. *PLoS Pathog* 15:e1007944. <https://doi.org/10.1371/journal.ppat.1007944>.
 54. McLellan JS, Pancera M, Carrico C, Gorman J, Julien J-P, Khayat R, Louder R, Pejchal R, Sastry M, Dai K, O'Dell S, Patel N, Shahzad-ul-Hussan S, Yang Y, Zhang B, Zhou T, Zhu J, Boyington JC, Chuang G-Y, Diwanji D, Georgiev I, Kwon YD, Lee D, Louder MK, Moquin S, Schmidt SD, Yang Z-Y, Bonsignori M, Crump JA, Kapiga SH, Sam NE, Haynes BF, Burton DR, Koff WC, Walker LM, Phogat S, Wyatt R, Orwenyo J, Wang L-X, Arthos J, Bewley CA, Mascola JR, Nabel GJ, Schief WR, Ward AB, Wilson IA, Kwong PD. 2011. Structure of HIV-1 gp120 V1/V2 domain with broadly neutralizing antibody PG9. *Nature* 480:336–343. <https://doi.org/10.1038/nature10696>.
 55. Yuan Y, Cao D, Zhang Y, Ma J, Qi J, Wang Q, Lu G, Wu Y, Yan J, Shi Y, Zhang X, Gao GF. 2017. Cryo-EM structures of MERS-CoV and SARS-CoV spike glycoproteins reveal the dynamic receptor binding domains. *Nat Commun* 8:15092. <https://doi.org/10.1038/ncomms15092>.
 56. Kwong PD, Wyatt R, Robinson J, Sweet RW, Sodroski J, Hendrickson WA. 1998. Structure of an HIV gp120 envelope glycoprotein in complex with the CD4 receptor and a neutralizing human antibody. *Nature* 393:648–659. <https://doi.org/10.1038/31405>.
 57. Escribano-Romero E, Rawling J, García-Barreno B, Melero JA. 2004. The soluble form of human respiratory syncytial virus attachment protein differs from the membrane-bound form in its oligomeric state but is still capable of binding to cell surface proteoglycans. *J Virol* 78:3524–3532. <https://doi.org/10.1128/jvi.78.7.3524-3532.2004>.
 58. Fuentes S, Coyle EM, Golding H, Khurana S. 2015. Nonglycosylated G-protein vaccine protects against homologous and heterologous respiratory syncytial virus (RSV) challenge, while glycosylated G enhances RSV lung pathology and cytokine levels. *J Virol* 89:8193–8205. <https://doi.org/10.1128/JVI.00133-15>.
 59. Cullen LM, Schmidt MR, Morrison TG. 2017. The importance of RSV F protein conformation in VLPs in stimulation of neutralizing antibody titers in mice previously infected with RSV. *Hum Vaccin Immunother* 13:2814–2823. <https://doi.org/10.1080/21645515.2017.1329069>.
 60. Krammer F, Pica N, Hai R, Tan GS, Palese P. 2012. Hemagglutinin stalk-reactive antibodies are boosted following sequential infection with seasonal and pandemic H1N1 influenza virus in mice. *J Virol* 86:10302–10307. <https://doi.org/10.1128/JVI.01336-12>.
 61. Hai R, Krammer F, Tan GS, Pica N, Eggink D, Maamary J, Margine I, Albrecht RA, Palese P. 2012. Influenza viruses expressing chimeric hemagglutinins: globular head and stalk domains derived from different subtypes. *J Virol* 86:5774–5781. <https://doi.org/10.1128/JVI.00137-12>.
 62. Krammer F, Pica N, Hai R, Margine I, Palese P. 2013. Chimeric hemagglutinin influenza virus vaccine constructs elicit broadly protective stalk-specific antibodies. *J Virol* 87:6542–6550. <https://doi.org/10.1128/JVI.00641-13>.
 63. Impagliazzo A, Milder F, Kuipers H, Wagner MV, Zhu X, Hoffman RMB, van Meersbergen R, Huizingh J, Wanningen P, Verspuij J, de Man M, Ding Z, Apetri A, Kükler B, Sneekes-Vriese E, Tomkiewicz D, Laursen NS, Lee PS, Zakrzewska A, Dekking L, Tolboom J, Tettero L, van Meerten S, Yu W, Koudstaal W, Goudsmit J, Ward AB, Meijberg W, Wilson IA, Radošević K. 2015. A stable trimeric influenza hemagglutinin stem as a broadly protective immunogen. *Science* 349:1301–1306. <https://doi.org/10.1126/science.aac7263>.
 64. Lu Y, Welsh JP, Swartz JR. 2014. Production and stabilization of the trimeric influenza hemagglutinin stem domain for potentially broadly protective influenza vaccines. *Proc Natl Acad Sci U S A* 111:125–130. <https://doi.org/10.1073/pnas.1308701110>.
 65. Pallesen J, Wang N, Corbett KS, Wrapp D, Kirchdoerfer RN, Turner HL, Cottrell CA, Becker MM, Wang L, Shi W, Kong WP, Andres EL, Kattenbach AN, Denison MR, Chappell JD, Graham BS, Ward AB, McLellan JS. 2017. Immunogenicity and structures of a rationally designed prefusion MERS-CoV spike antigen. *Proc Natl Acad Sci U S A* 114:E7348–E7357. <https://doi.org/10.1073/pnas.1707304114>.
 66. Stewart-Jones GBE, Chuang GY, Xu K, Zhou T, Acharya P, Tsybovsky Y, Ou

- L, Zhang B, Fernandez-Rodriguez B, Gilardi V, Silacci-Fregni C, Beltramello M, Baxa U, Druz A, Kong WP, Thomas PV, Yang Y, Foulds KE, Todd JP, Wei H, Salazar AM, Scropio DG, Carragher B, Potter CS, Corti D, Mascola JR, Lanzavecchia A, Kwong PD. 2018. Structure-based design of a quadrivalent fusion glycoprotein vaccine for human parainfluenza virus types 1-4. *Proc Natl Acad Sci U S A* 115:12265–12270. <https://doi.org/10.1073/pnas.1811980115>.
67. McLellan JS, Chen M, Joyce MG, Sastry M, Stewart-Jones GB, Yang Y, Zhang B, Chen L, Srivatsan S, Zheng A, Zhou T, Graepel KW, Kumar A, Moin S, Boyington JC, Chuang GY, Soto C, Baxa U, Bakker AQ, Spits H, Beaumont T, Zheng Z, Xia N, Ko SY, Todd JP, Rao S, Graham BS, Kwong PD. 2013. Structure-based design of a fusion glycoprotein vaccine for respiratory syncytial virus. *Science* 342:592–598. <https://doi.org/10.1126/science.1243283>.
68. Krarup A, Truan D, Furmanova-Hollenstein P, Bogaert L, Bouchier P, Bisschop IJ, Widjojatmodjo MN, Zahn R, Schuitemaker H, McLellan JS, Langedijk JP. 2015. A highly stable prefusion RSV F vaccine derived from structural analysis of the fusion mechanism. *Nat Commun* 6:8143. <https://doi.org/10.1038/ncomms9143>.
69. Qiao H, Pelletier SL, Hoffman L, Hacker J, Armstrong RT, White JM. 1998. Specific single or double proline substitutions in the “spring-loaded” coiled-coil region of the influenza hemagglutinin impair or abolish membrane fusion activity. *J Cell Biol* 141:1335–1347. <https://doi.org/10.1083/jcb.141.6.1335>.
70. Sanders RW, Vesanan M, Schuelke N, Master A, Schiffner L, Kalyanaraman R, Paluch M, Berkhout B, Maddon PJ, Olson WC, Lu M, Moore JP. 2002. Stabilization of the soluble, cleaved, trimeric form of the envelope glycoprotein complex of human immunodeficiency virus type 1. *J Virol* 76:8875–8889. <https://doi.org/10.1128/jvi.76.17.8875-8889.2002>.
71. Battles MB, Mas V, Olmedillas E, Cano O, Vazquez M, Rodriguez L, Melero JA, McLellan JS. 2017. Structure and immunogenicity of pre-fusion-stabilized human metapneumovirus F glycoprotein. *Nat Commun* 8:1528. <https://doi.org/10.1038/s41467-017-01708-9>.
72. Battye TG, Kontogiannis L, Johnson O, Powell HR, Leslie AG. 2011. iMOSFLM: a new graphical interface for diffraction-image processing with MOSFLM. *Acta Crystallogr D Biol Crystallogr* 67:271–281. <https://doi.org/10.1107/S0907444910048675>.
73. Evans PR, Murshudov GN. 2013. How good are my data and what is the resolution? *Acta Crystallogr D Biol Crystallogr* 69:1204–1214. <https://doi.org/10.1107/S0907444913000061>.
74. McCoy AJ, Grosse-Kunstleve RW, Adams PD, Winn MD, Storoni LC, Read RJ. 2007. Phaser crystallographic software. *J Appl Crystallogr* 40: 658–674. <https://doi.org/10.1107/S0021889807021206>.
75. Adams PD, Afonine PV, Bunkoczi G, Chen VB, Davis IW, Echols N, Headd JJ, Hung LW, Kapral GJ, Grosse-Kunstleve RW, McCoy AJ, Moriarty NW, Oeffner R, Read RJ, Richardson DC, Richardson JS, Terwilliger TC, Zwart PH. 2010. PHENIX: a comprehensive Python-based system for macromolecular structure solution. *Acta Crystallogr D Biol Crystallogr* 66:213–221. <https://doi.org/10.1107/S0907444909052925>.
76. Emsley P, Cowtan K. 2004. Coot: model-building tools for molecular graphics. *Acta Crystallogr D Biol Crystallogr* 60:2126–2132. <https://doi.org/10.1107/S0907444904019158>.